An upconversion NaYF$_4$:Yb^{3+},Er^{3+}/TiO$_2$ core−shell nanoparticle photoelectrode for improved efficiencies of dye-sensitized solar cells

Jun Zhang [a,*], Haiou Shen [a], Wei Guo [b], Shunhao Wang [a], Chuntao Zhu [a], Fang Xue [a], Jinfeng Hou [c], Haiquan Su [a], Zhuobin Yuan [d]

[a] School of Chemistry and Chemical Engineering, Inner Mongolia University, 235 West University Road, Hohhot 010021, China
[b] College of Environmental and Resource Sciences, Inner Mongolia University, Hohhot 010021, China
[c] Test Center, Inner Mongolia University of Technology, Hohhot 010051, China
[d] College of Chemistry and Chemical Engineering, Graduate University of the Chinese Academy of Sciences, Beijing 100049, China

HIGHLIGHTS

► NaYF$_4$:Yb^{3+},Er^{3+}/TiO$_2$ core−shell nanoparticles as the photoelectrode of DSSCs.
► It can convert infrared to visible luminescence and retain semiconductor character.
► The DSSCs with this core−shell appeared the best photoelectric performances.

GRAPHICAL ABSTRACT
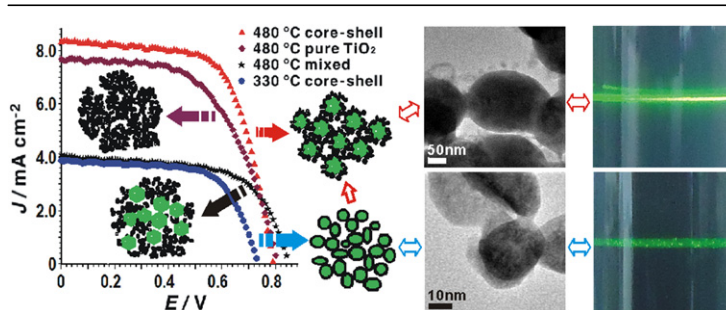
ABSTRACT

Novel upconversion NaYF$_4$:Yb^{3+},Er^{3+}/TiO$_2$ core−shell nanoparticles (NPs) are synthesized and used to prepare the photoelectrode (PE) of dye-sensitized solar cells (DSSCs). The morphology, structure, photoluminescence characterization of the NaYF$_4$:Yb^{3+},Er^{3+}/TiO$_2$ core−shell NPs and the photoelectric performance, alternating current impedance spectroscopy of DSSCs are characterized using transmission electron microscopy, X-ray diffraction, upconversion luminescence (UCL) spectrofluorimetry and electrochemistry. Compared with the pure TiO$_2$ PE or the NaYF$_4$:Yb^{3+},Er^{3+} upconversion NPs and TiO$_2$ simply mixed prepared PE as the volume ratio of the core−shell structure, the DSSCs with the upconversion core−shell PE show a greater photovoltaic efficiency. The energy conversion efficiency of the DSSCs with a NaYF$_4$:Yb^{3+},Er^{3+}/TiO$_2$ PE is 23.1% higher than with a pure TiO$_2$ PE and 99.1% higher than with a mixed PE using the same conditions. This enhancement is due to the UCL core extending the spectral response range of DSSCs to the infrared region and their particular shell structure, retaining its semiconductor character. This method represents a novel approach to increase the efficiencies of DSSCs.

© 2012 Elsevier B.V. All rights reserved.

1. Introduction

Clean, renewable energy utilization has recently been proposed as a main solution for global warming [1]. A dye-sensitized solar cells (DSSCs), first designed by O'Reagan and Gratzel in 1991 [2], is a remarkable renewable energy system with low cost and a simple fabrication methodology. A DSSC comprises a photoelectrode (PE) of dye adsorbed on porous nanocrystalline TiO$_2$, a counter electrode of platinum or conductive polymer [3] and an electrolyte solution between the electrodes. The PE is one of the most important components in the DSSC because the amount of light absorbed in

the DSSC is dependent on the absorption spectrum of the PE [4]. Generally, DSSCs with a dye-sensitized TiO_2 PE have a maximum absorption in the visible region of the total incident solar irradiation [5,6], which means that approximately 50% of solar irradiation energy in the ultraviolet and infrared regions is not utilized [7]; therefore, the solar energy conversion efficiency of DSSCs is limited in these cases [8]. Accordingly, extending the spectral response range of DSSCs to the infrared or ultraviolet region is extremely important to increase the efficiency of DSSCs.

Upconversion, lanthanide-based NPs have received considerable attention because they can convert near-infrared (NIR) photons to visible light by absorbing low-energy photons and then emitting high-energy photons. They have been extensively studied to be used in flat-panel displays [9], solar cells [10], iatrical detection [11] and bio-imaging probes [12–14] because of advantages such as their upconversion luminescence (UCL) characteristics, high light penetration depth in tissues, no photo damage to living organisms and low background noise. Hexagonal phase sodium yttrium fluoride (β-$NaYF_4$) crystals have been reported to be one of the most efficient upconversion host materials and have been widely studied [15,16]. The hexagonal phase $NaYF_4$:Yb^{3+},Er^{3+} core is the most efficient NIR-to-visible UCL material and exhibits a strong upconversion fluorescence [17–19]. In addition, the core–shell geometry makes possible the combination of core and shell characteristics, which further improves the function of devices and expands the range of potential applications. Practically, much effort has gone into the design and fabrication of nanocomposites with a core–shell structure [20–23]. To our knowledge, however, the usage of $NaYF_4$:Yb^{3+},Er^{3+}/TiO_2 core–shell structure in DSSCs has not yet been reported in the literature.

In this work, a multifunctional $NaYF_4$:Yb^{3+},Er^{3+}/TiO_2 core–shell structured nanocomposite was synthesized and used as a PE of DSSCs to investigate the possibility of increasing the spectral response of DSSCs for the first time. The combination of UCL materials and the TiO_2 semiconductor not only has upconversion properties but also functions as a semiconductor. The morphology, structure and photoluminescence properties of the $NaYF_4$:Yb^{3+},Er^{3+}/TiO_2 core–shell nanoparticles (NPs) and the photoelectric performance and alternating current (AC) impedance spectroscopy of DSSCs were characterized by transmission electron microscopy (TEM), X-ray diffraction (XRD), upconversion luminescence (UCL) spectrofluorimetry and electrochemistry. The enhancement of the photovoltaic efficiency of the novel upconversion core–shell PE of DSSCs was also investigated.

2. Experimental

2.1. Synthesis of $NaYF_4$:Yb^{3+},Er^{3+} UCL NPs

$NaYF_4$:Yb^{3+},Er^{3+} UCL NPs were synthesized in oleylamine (OM) by thermolysis of rare earth trifluoroacetates (($CF_3COO)_3RE$) and sodium trifluoroacetate (CF_3COONa) precursors [24,25]. Y_2O_3 (0.39 mmol), Na_2CO_3 (0.50 mmol), Yb_2O_3 (0.10 mmol) and Er_2O_3 (0.01 mmol) were dissolved in 10 mL of 50% aqueous trifluoroacetic acid at 80 °C. The trifluoroacetates were obtained from the slow evaporation of the residual water and acid. Then, 10 mL of OM was added. The reaction solution was heated to 120 °C and maintained at this temperature for 30 min to remove residual water and oxygen, during which the flask was purged periodically with dry argon. The resulting optically transparent solution was heated to 330 °C and maintained at this temperature for 1 h under an argon atmosphere to prepare $NaYF_4$:Yb^{3+},Er^{3+} UCL NPs. After this period, the reaction solution was cooled down to 80 °C $NaYF_4$:Yb^{3+},Er^{3+} UCL NPs were precipitated by the addition of absolute ethanol. The products were isolated by centrifugation and washed with hexane

and deionized water. This procedure was repeated at least two more times. The resulting UCL NPs were dispersed in 25 mL of 5 mM cetyltrimethyl ammonium bromide (CTAB) isopropyl alcohol solution and stirred for 1 h. In the solution obtained, CTAB was absorbed to the surface of the $NaYF_4$:Yb^{3+},Er^{3+} UCL NPs as the cationic surfactants [26], causing the surface of the UCL NPs to become positive.

2.2. Synthesis of $NaYF_4$:Yb^{3+},Er^{3+}/TiO_2 core–shell NPs

The preparation of multifunctional $NaYF_4$:Yb^{3+},Er^{3+}/TiO_2 core–shell NPs was as follows: an 18 mL of 8.2 mM isopropyl titanate isopropyl alcohol solution mixing with the same molecular acetylacetone (1:1, the molar ratio with the isopropyl titanate) served as the TiO_2 precursor [27]. Then, 6 mL 50% isopropanol aqueous solution was added drop by drop under strong stirring. The reaction solution was heated to 80 °C and the prepared UCL NPs isopropyl alcohol solution containing CTAB was added. After the addition of 0.03 g of ammonium persulfate, the solution was refluxed at 80 °C for 90 min. A TiO_2 shell was formed on the surface of the UCL NPs. The products were isolated by centrifugation and washed three times with absolute ethanol and deionized water.

2.3. Synthesis of TiO_2 NPs

The TiO_2 NPs were synthesized using sol–gel and hydrolysis techniques from tetrabutyl titanate (97 wt%) precursor [28]. The typical preparation process was as follows: Tetrabutyl titanate was hydrolyzed in a pH = 3 ethanol aqueous solution under strong stirring, then dried at 80 °C in an oven for 2 h.

2.4. DSSC fabrication

$NaYF_4$:Yb^{3+},Er^{3+}/TiO_2 core–shell NPs were used for slurry. The film electrodes were fabricated via the doctor-blade technique on FTO glass (14 Ω sq^{-1}, an average transmittance of 90% in the visible wavelength, Nippon Sheet Glass Co., Japan, active area = 0.196 cm^2) [29]. After air drying, the electrodes for the DSSCs were annealed for 30 min at 100 °C, 330 °C and 480 °C and treated with a 0.1 M $TiCl_4$ aqueous solution at 70 °C for 1 h. Following annealing for 30 min at 100 °C, 330 °C and 480 °C, the electrodes were immersed in a 0.5 mM solution of cis-bis(isothiocyanato)bis(2,2′-bipyridyl-4,4′-dicarboxylato)-ruthenium(II)-bis-etrabutyl ammonium (N719 dye, Solaronix) in ethanol for 24 h at room temperature in the dark [3]. Finally, a dye-sensitized solar cell was assembled by injecting a drop of electrolyte containing 0.05 M I_2, 0.5 M LiI, 0.6 M 1,2-dimethyl-3-propylimidazolium iodide, 0.5 M guanidine thiocyanate, and 0.5 M 4-tert-butylpyridine in 10 mL acetylacetone into the aperture between the $NaYF_4$:Yb^{3+},Er^{3+}/TiO_2 PE and a platinized FTO glass counter electrode. The DSSC based on a pure TiO_2 electrode or $NaYF_4$:Yb^{3+},Er^{3+} and TiO_2 NPs (volume ratio similar to the core–shell) mixed electrode was prepared using the same method.

2.5. Characterization

TEM was used to study the NP morphology. TEM measurements were performed on a JEM-2010 (JEOL) microscope operated at 200 kV. Powder X-ray diffraction patterns were measured by XD-3 X-ray diffraction with Cu K_α radiation (K_α = 0.15406 nm) at 36 kV and 20 mA. Upconversion spectra of the core and core–shell NPs were detected using a FLS920 fluorescence spectrophotometer. A 980 nm diode laser (0.8 W) was used when measuring the samples.

The photovoltaic testing of the DSSCs was performed by measuring the photocurrent density-cell potential curves using a CHI660C electrochemical device under simulated AM 1.5 solar

illumination at 100 mW cm^{-2} from a xenon lamp in ambient atmosphere before and after using an IR-cut filter (750 ± 5 nm at $T = 50\%$, 400–720 nm at $T > 85\%$, 780–1100 nm at $T < 0.1\%$, Giai-photonics Co., China). The fill factor and overall light-to-electrical energy conversion efficiency of the DSSCs were calculated according to the equations in reference [30]. AC impedance spectra of the DSSCs with different PEs were measured using a CHI660C electrochemical device assembled with a platinized FTO glass electrode as the counter electrode under simulated AM 1.5 solar illumination at 100 mW cm^{-2} from a xenon lamp in an ambient atmosphere. Initial E = open-circuit voltage of each cell, high frequency = 1×10^5 Hz, low frequency = 0.05 Hz, amplitude = 0.005 V, and quiet time = 2 s.

3. Results and discussion

3.1. Morphology and structure characterizations

Fig. 1 shows the TEM images of TiO$_2$ and NaYF$_4$:Yb^{3+},Er^{3+}/TiO$_2$ core–shell NPs at different annealing temperatures. When annealed at 100 °C (Fig. 1a), the TiO$_2$ NPs were determined to be approximately 10–20 nm in diameter. At higher annealing temperatures (Fig. 1b, c), the TiO$_2$ NPs agglomerated to 20–30 nm in size at 330 °C and greater than 30 nm with numerous approximately 10 nm particles at 480 °C. Meanwhile, the TiO$_2$ agglomeration changed from homogeneous at 330 °C to heterogeneous at 480 °C, which could be due to the changing of the crystal lattice or the loss of residual water molecules and organic groups during the annealing process.

The core–shell structures of the NaYF$_4$:Yb^{3+},Er^{3+}/TiO$_2$ core–shell NPs annealed at 100 °C, 330 °C and 480 °C were clearly observed in the TEM images shown in Fig. 1d–l. As the annealing temperature increased, the shell changed from uniform TiO$_2$ lamella to disrupted TiO$_2$ NPs enwrapping the NaYF$_4$:Yb^{3+},Er^{3+} core. The TEM image shows that the TiO$_2$ shell was thin and uniform, with a thickness of approximately 3–4 nm, which is much smaller than the diameter of the NaYF$_4$:Yb^{3+},Er^{3+} NPs annealed at 100 °C (Fig. 1e, in circle). After annealing at 330 °C, the TiO$_2$ shell of the NaYF$_4$:Yb^{3+},Er^{3+}/TiO$_2$ core–shell became thicker and irregular: it had a thicker shell on part of the particles and a thinner shell on most of the particles (Fig. 1h, in circle). Moreover, some sections of the outermost layer of the TiO$_2$ shell chapped and formed a shell of 10–30 nm TiO$_2$ NPs enwrapping the NaYF$_4$:Yb^{3+},Er^{3+} core (refer to the arrows in Fig. 1k, l). At some areas of the core surface, the TiO$_2$ shell became much thinner, such that the NaYF$_4$:Yb^{3+},Er^{3+} core was almost bare; light was easily transmitted at these areas. This result was likely due to two factors in the shell's structural evolvement: the change of the crystallite shape of the TiO$_2$ shell and the increase in the NaYF$_4$:Yb^{3+},Er^{3+} core size [31]. The shell annealed at 100 °C was composed of lots of dispersing crystalline regions with the lattice spacing from 0.342 nm to 0.354 nm determined by a selected area fast Fourier transform (FFT) pattern (the inset of Fig. 1f). The lattice arrangement of the shell annealed at 330 °C was regular with a lattice spacing of 0.351 nm (also determined by the FFT pattern in the inset of Fig. 1i) and corresponded to the lattice spacing of the {101} plane of the anatase phase. For the NaYF$_4$:Yb^{3+},Er^{3+} core annealed at 100 °C and 330 °C (Fig. 1d–h), most particles observed were approximately 20–40 nm in size and coexisted with a few smaller size particles; however, the size of the NaYF$_4$:Yb^{3+},Er^{3+} core annealed at 480 °C (Fig. 1j, k) increased to 100–150 nm. The increase in the core size could also be advantageous for the shell's morphological and structural evolution as the annealing temperature is increased.

Fig. 2 shows the crystalline structures of the NaYF$_4$:Yb^{3+},Er^{3+}/TiO$_2$ core–shell (Fig. 2a), the NaYF$_4$:Yb^{3+},Er^{3+} core (Fig. 2b) and the

TiO$_2$ NPs (Fig. 2c) characterized using the powder XRD technique. Anatase phase gradually formed in the TiO$_2$ NPs (Fig. 2c) when the annealing temperature increased from 100 °C to 330 °C and completely transformed into pure anatase when annealed at 480 °C, as determined from the appearance of the anatase TiO$_2$ peaks confirmed by the Joint Committee on Powder Diffraction Standards Card File No. 21-1272 (JCPDS 21-1272) from 100 °C to 330 °C and the disappearance of non anatase diffraction peaks (Fig. 2c, arrows) from 330 °C to 480 °C. From the XRD pattern of the NaYF$_4$:Yb^{3+},Er^{3+} core in Fig. 2b, the samples were observed to be well crystallized, and the diffraction peaks matched the standard pattern of the highly crystalline hexagonal phase of the NaYF$_4$:Yb^{3+},Er^{3+} crystals (JCPDS 28-1192) at different annealing temperatures, with the exception of a small presence of NaF impurity in the sample at 480 °C (Fig. 2b, arrows). From Fig. 2a–c, the diffraction peaks of the crystalline hexagonal phase of the NaYF$_4$:Yb^{3+},Er^{3+} core and the TiO$_2$ shell with anatase characteristics were observed simultaneously. From the XRD patterns of NaYF$_4$:Yb^{3+},Er^{3+}/TiO$_2$ core–shell annealed at 330 °C, diffraction peaks of anatase TiO$_2$ were observed beside the crystalline hexagonal phase NaYF$_4$:Yb^{3+},Er^{3+} core diffraction peaks, which confirmed the coexistence of the core and shell, as shown in Fig. 1h and i. For the NaYF$_4$:Yb^{3+},Er^{3+}/TiO$_2$ core–shell annealed at 480 °C, the diffraction peaks of the NaYF$_4$:Yb^{3+},Er^{3+}/TiO$_2$ core were weaker, and the diffraction peaks of the anatase TiO$_2$ shell were higher and sharper than at 330 °C, indicating that the bulky core formed and thus weakened the contribution of the unit volume core. The shell remained as anatase TiO$_2$, and the anatase TiO$_2$ surface exposure was increased according to the structural change of the core and shell, as shown in Fig. 1j–l. The 27.8° peak (Fig. 2a, arrow) was a sign of rare earth elements in combination with titanium sodium compounds (Na$_5$Ti$_3$F$_{14}$, JCPDS 27-0816) and indicated that the TiO$_2$ shell and the NaYF$_4$:Yb^{3+},Er^{3+} NP core were chemically combined and not mixed or in simple contact in the core–shell structure at 480 °C, as shown in Fig. 1j–l.

3.2. Photoluminescence characteristics (PL)

Fig. 3 shows the room temperature upconversion fluorescence spectra of NaYF$_4$:Yb^{3+},Er^{3+} and NaYF$_4$:Yb^{3+},Er^{3+}/TiO$_2$ core–shell NPs in powder and their photographs in solution under NIR excitation (980 nm). The visible luminescence spectrum of the NaYF$_4$:Yb^{3+},Er^{3+} NPs reveals two emission bands in the green (525, 542 nm) and red (655 nm) spectral regions (Fig. 3e), which can be attributed to the $^2H_{11/2}$,$^4S_{3/2}$–$^4I_{15/2}$ (green) and $^4F_{9/2}$–$^4I_{15/2}$ (red) transitions of Er^{3+} ions [11,31]. The intensity of the green emission is stronger than that of the red emission. From 100 °C to 480 °C, the fluorescence intensity of the NaYF$_4$:Yb^{3+},Er^{3+} core was gradually enhanced (Fig. 3e–h), which appeared green rather than red because the human naked eye is more sensitive to green color than red, as shown in these photographs.

After the NaYF$_4$:Yb^{3+},Er^{3+} NPs were coated with a TiO$_2$ layer, their visible luminescence spectrum retained the same emission bands as the cores, and the fluorescence intensity decreased to some extent because of the light-reflecting, light-refracting and light-scattering effect on both the emission and incident light by the TiO$_2$ layer (Fig. 3a). It is well recognized that the emission of rare earth ions will be quenched to some extent in the environments that have a high phonon frequency [32]. The organic groups in CTAB that have tremendous vibration frequencies from 1000 to 3500 cm^{-1} will quench the emission of Er^{3+} to a great extent in the NaYF$_4$:Yb^{3+},Er^{3+}/TiO$_2$ core–shell system for 100 °C and 330 °C. The penetrability of a long wave is known to be superior to a shorter wave. For 100 °C and 330 °C, the short wave part of the green spectral region (525, 542 nm) was mostly quenched by CTAB and
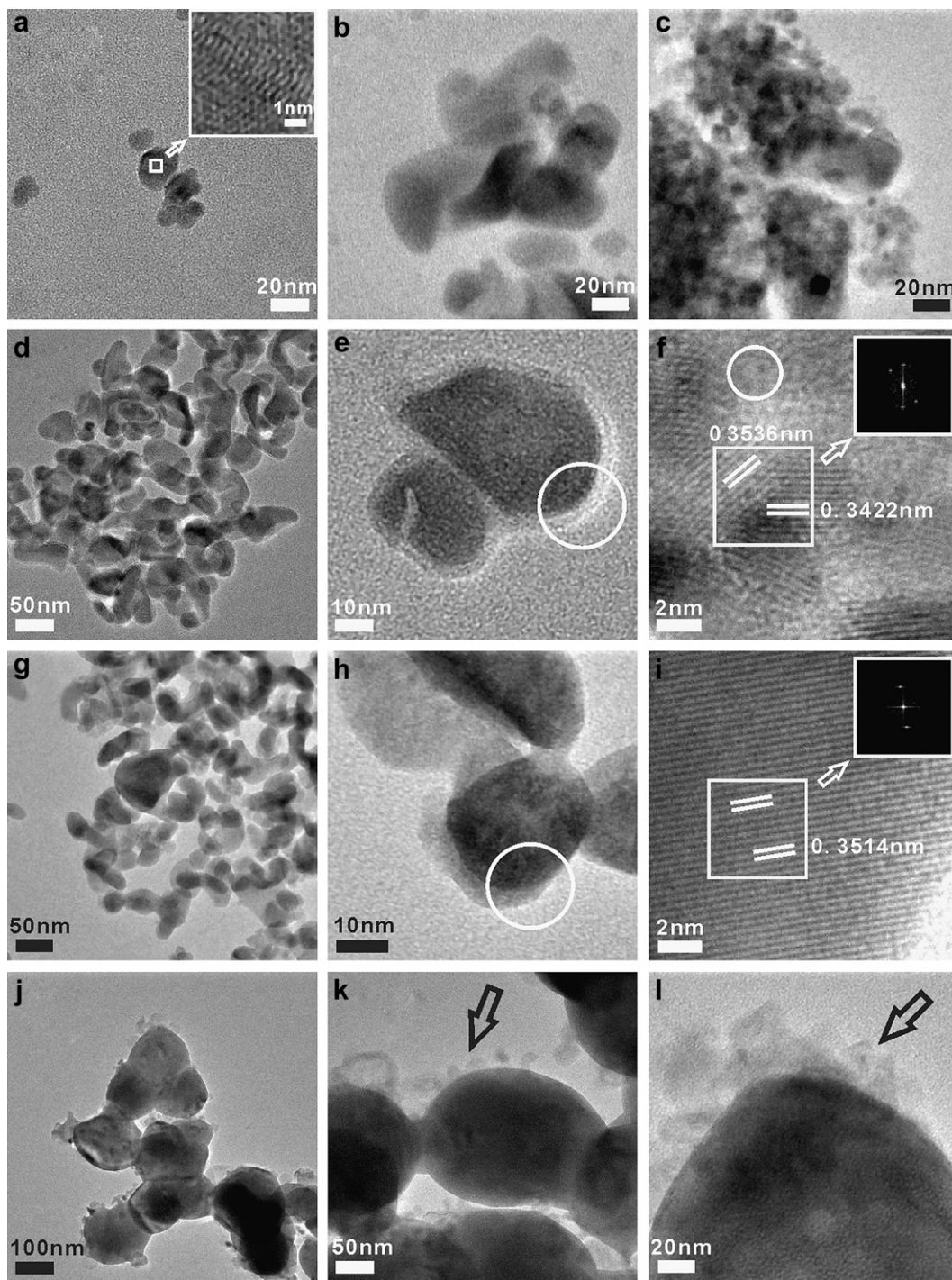
Fig. 1. TEM images of TiO$_2$ NPs annealed at (a) 100 °C, (b) 330 °C and (c) 480 °C and NaYF$_4$:Yb^{3+},Er^{3+}/TiO$_2$ core–shell NPs annealed at (d–f) 100 °C, (g–i) 330 °C and (j–l) 480 °C with bars of different scales. The insets show the fast Fourier transform (FFT) patterns of the selected areas in (f) and (i).

then the remainder reflected by the tight TiO$_2$ shell and severely weakened, with only wavelengths greater than 660 nm partly penetrating the shell. Very faint emissions visible to the naked eye could be detected under an NIR laser, as shown in Fig. 3b and c. However, the fluorescence intensity of the core–shell annealed at 480 °C became remarkably strong (Fig. 3d) due to the TiO$_2$ shell chapping (Fig. 1j–l) and the residual CTAB being removed with its thermal decomposition. In addition, with the increase in temperature, the size of the particles became larger, which could

remarkably increase the fluorescence intensity of the core [33]. The gradually enhanced fluorescence intensity of the NaYF$_4$:Yb^{3+},Er^{3+}/TiO$_2$ core–shell with annealing temperature can be seen in Fig. 3a–d. Moreover, upon comparison of Fig. 3a with Fig. 3e, the intensity ratio of the green emission to the red emission was reduced after coating with the TiO$_2$ shell, which may due to the presence of a shell that changes some energy gap bridges that facilitate the nonradiative energy transfer of $^4I_{13/2}$–$^4F_{9/2}$ and $^4I_{15/2}$–$^4I_{11/2}$ for Er^{3+} [11].
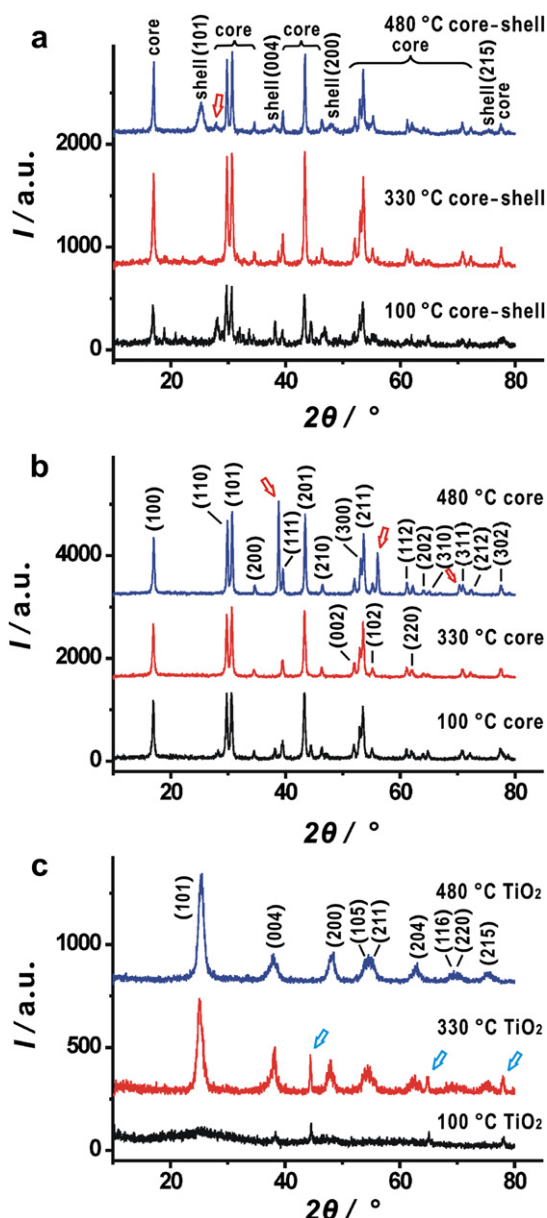
Fig. 2. XRD patterns of the (a) $NaYF_4:Yb^{3+},Er^{3+}/TiO_2$ core−shell, (b) $NaYF_4:Yb^{3+},Er^{3+}$ core and (c) TiO_2 NPs annealed at different temperatures.

Fig. 3. Upconversion fluorescence spectra of the (a) $NaYF_4:Yb^{3+},Er^{3+}/TiO_2$ core−shell and (e) $NaYF_4:Yb^{3+},Er^{3+}$ core NPs annealed at 100 °C, 330 °C or 480 °C (the insets are enlarged sections of the graphs) and their photographs: (b) 100 °C, (c) 330 °C and (d) 480 °C core−shell; (f) 100 °C, (g) 330 °C and (h) 480 °C core. All samples were excited with a 980 nm laser diode.

3.3. Photoelectric performance of DSSCs with different PEs

Fig. 4 shows the photoelectric performance of DSSCs using the $NaYF_4:Yb^{3+},Er^{3+}/TiO_2$ core−shell, mixed and pure TiO_2 PEs. The best photoelectric properties occurred after annealing at 480 °C. Here, the short-circuit photocurrent density (J_{sc}), fill factors (FF) and photoelectric conversion efficiency (η) of the $NaYF_4:Yb^{3+},Er^{3+}/TiO_2$ core−shell PE were found to be higher than those of both the pure TiO_2 and mixed PEs that were formed with the same annealing temperature (480 °C). However, the open-circuit voltage (V_{oc}) of the mixed PE was the highest among these electrodes (listed in Table 1). The energy conversion efficiency of the DSSCs with a $NaYF_4:Yb^{3+},Er^{3+}/TiO_2$ core−shell PE annealed at 480 °C was 23.1% higher than with a pure TiO_2 PE and 99.1% higher than with a mixed PE using the same conditions due to the special $NaYF_4:Yb^{3+},Er^{3+}/TiO_2$ core−shell structure, which extended the spectral response range of the DSSC and improved the light utilization rate of the
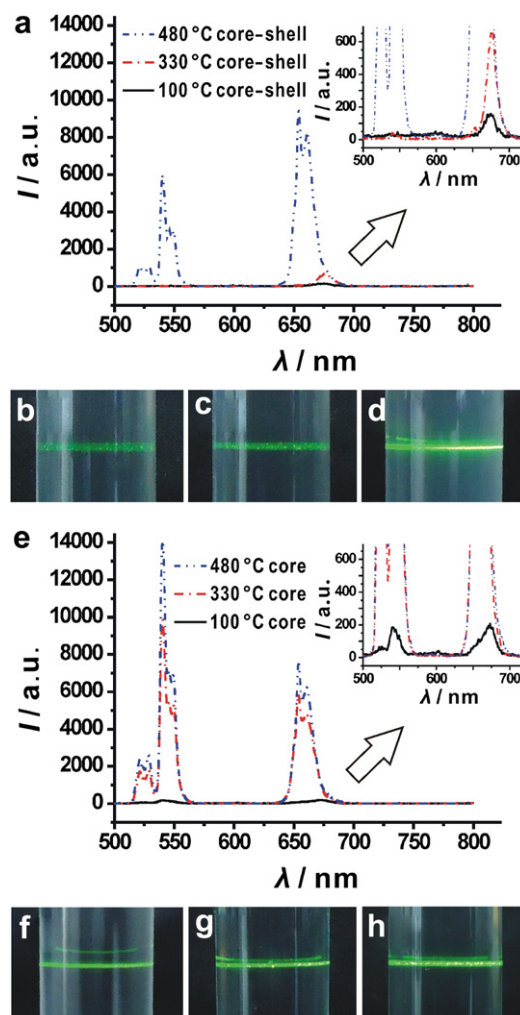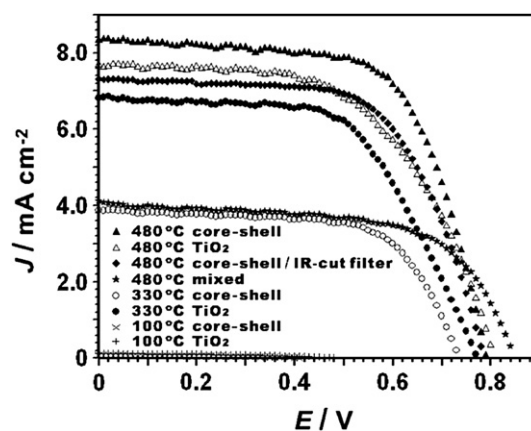

Fig. 4. Photocurrent density (j)−cell potential (E) curves of the DSSCs based on pure TiO_2 and $NaYF_4:Yb^{3+},Er^{3+}/TiO_2$ core−shell PEs annealed at 100 °C, 330 °C and 480 °C and the mixed PE annealed at 480 °C measured before using the IR-cut filter, and the $NaYF_4:Yb^{3+},Er^{3+}/TiO_2$ core−shell PE annealed at 480 °C measured after using the IR-cut filter. The measurements were recorded under 100 mW cm^{-2} illumination using linear sweep voltammetry with an initial $E = 0$ V, a final $E = 0.9$ V and a scan rate = 25 mV s^{-1}.

Table 1
The photovoltaic parameters of the DSSCs based on the pure TiO_2 and $NaYF_4$:Yb^{3+},Er^{3+}/TiO_2 core–shell PEs annealed at 100 °C, 330 °C and 480 °C and the mixed PE annealed at 480 °C measured before using the IR-cut filter, and the $NaYF_4$:Yb^{3+},Er^{3+}/TiO_2 core–shell PE annealed at 480 °C measured after using the IR-cut filter.

Electrode	J_{sc}/mA cm^{-2}	V_{oc}/V	FF	η/%
100 °C pure TiO_2	0.119	0.481	0.41	0.02
330 °C pure TiO_2	6.821	0.773	059	3.12
480 °C pure TiO_2	7.684	0.806	0.56	3.51
100 °C core–shell	0.063	0.419	0.38	0.01
330 °C core–shell	3.876	0.736	0.65	1.85
480 °C core–shell	8.321	0.791	0.66	4.32
480 °C core–shell/IR-cut filter	7.321	0.785	0.64	3.66
480 °C mixed	4.082	0.849	0.63	2.17

DSSC as a result of the $NaYF_4$:Yb^{3+},Er^{3+} core. Additionally, the TiO_2 shell endowed the core–shell NPs with the TiO_2 nature. The TiO_2 net structure remains in the PE, as shown in Fig. 1j and k, which could be the intrinsic reason why the core–shell PE performed so well comparing with the mixed PE. In the latter the TiO_2 net structure was destroyed owing to the accumulation of nonconductor $NaYF_4$:Yb^{3+},Er^{3+} NPs. The electron transfer was often blocked in the mixed PE and resulted in the lowest J_{sc} and η of DSSCs. In order to identify that the enhancement of solar cell efficiency was due to nothing else than upconversion, an IR-cut filter which can eliminate the light with wavelengths longer than 750 nm was used to measure the photoelectric properties of the $NaYF_4$:Yb^{3+},Er^{3+}/TiO_2 core–shell PE annealed at 480 °C. As shown in Fig. 4 and listed in Table 1, before and after using the IR-cut filter, the energy conversion efficiency of the DSSC was improved about 18.1%. It evidences that the long-wavelength light really contributes to increasing the DSSCs' efficiency due to upconversion.

The photoelectric performances of DSSCs with the $NaYF_4$:Yb^{3+},Er^{3+}/TiO_2 core–shell and pure TiO_2 PEs at different annealing temperatures are shown in Fig. 4. As the annealing temperature increased, the residual water or organic molecules in the NPs would burn off, and the NPs would link more closely to each other during the annealing process. The electron transfer resistance in NPs would decrease, and the photoelectric performances of the DSSCs would increase, whether with the $NaYF_4$:Yb^{3+},Er^{3+}/TiO_2 core–shell or pure TiO_2 PE [34]. However, the J_{sc}, V_{oc}, FF and η of DSSCs based on the $NaYF_4$:Yb^{3+},Er^{3+}/TiO_2 PE at 100 °C and 330 °C were all found to be lower than those measured with the pure TiO_2 PE. This result may be attributed to the non-conducting $NaYF_4$:Yb^{3+},Er^{3+} core and the residual CTAB in the tight TiO_2 shell for the $NaYF_4$:Yb^{3+},Er^{3+}/TiO_2 PE. Charge transfer was only permitted to take place in the TiO_2 shell, which weakened the conductivity of the NPs. In addition, UCL, especially the short wave part of the green spectral region (525, 542 nm), was severely weakened by the residual CTAB and tight TiO_2 shell (Fig. 3a). In fact, the absorption range of the N719 dye in the green spectral region (~500–600 nm) was more effective in the photoelectric performances of DSSCs than that in the red spectral region (655–660 nm) [35]. Here, the increase in the photoelectric performances by upconversion of the core was a secondary factor when compared with the counter effectiveness of the non-conductive core. Together, lower photoelectric performances than those of pure TiO_2 PE at 100 °C and 330 °C were obtained. When the annealing temperature was increased to 480 °C, the new structure of small TiO_2 NPs enwrapping a large UCL NP core (Fig. 1k, l) gradually formed in the $NaYF_4$:Yb^{3+},Er^{3+}/TiO_2 PE. UCL, especially the short wave part of the green spectral region (525, 542 nm) could resume and transmit easily through its new NP shell. As such, the increase in photoelectric performances by upconversion of the core became

the primary factor in comparison with the counter effectiveness of a non-conductive core; the J_{sc}, FF and η of DSSCs based on $NaYF_4$:Yb^{3+},Er^{3+}/TiO_2 PE are all higher than those of the pure TiO_2 PE (listed in Table 1).

3.4. AC impedance spectra of DSSCs with different PEs

AC impedance spectroscopy is a powerful method for investigating internal resistances and charge transfer processes in electrochemical systems. The intermediate-frequency feature is attributed to the electron transfer resistance at the PEs [36]. The AC impedance spectra in Fig. 5 clearly show the semicircles in the intermediate-frequency region, ranging from several thousands Hz to 1 Hz for the CEs studied. The impedance values around 10 Hz for different PEs indicate that the electron transfer resistance for the $NaYF_4$:Yb^{3+},Er^{3+} and TiO_2 mixed PE annealed at 480 °C was higher than those for the core–shell PE and the pure TiO_2 PE at the same annealing temperature, which may be attributed to the nonconductive $NaYF_4$:Yb^{3+},Er^{3+} NPs and the discontinuity of the TiO_2 in the mixed PE, and the core–shell PE was higher than the pure TiO_2 PE at the same annealing temperature.

Fig. 5 shows that as the temperature increases from 100 °C to 480 °C, the impedance values around 10 Hz decrease for the pure TiO_2 PEs, as do those for the core–shell PEs from 100 °C to 330 °C. It should be attributed to the TiO_2 NPs or shells of PEs becoming more tightly connected with the organic impurity decomposing at the high temperature. For the core–shell PEs annealed at 480 °C, however, the non-conductive core grew lager, and the shell became small TiO_2 NPs or even discontinuous, such that the electron transfer was negatively affected.

3.5. Investigation of the formation mechanism and function of the new core–shell PE

Scheme 1 shows the structural schematics of PEs based on a $NaYF_4$:Yb^{3+},Er^{3+}/TiO_2 core–shell and mixed and pure TiO_2 NPs, all annealed at 480 °C. The $NaYF_4$:Yb^{3+},Er^{3+}/TiO_2 core–shell structure that was annealed at 480 °C showed an excellent capacity of converting infrared to visible luminescence and retained its semiconductor character. When the annealing temperature increased from 100 °C to 480 °C, combining larger particles were formed, the TiO_2 shell of the $NaYF_4$:Yb^{3+},Er^{3+}/TiO_2 core–shell transformed from uniform TiO_2 lamella to disrupt TiO_2 NPs enwrapping the $NaYF_4$:Yb^{3+},Er^{3+} core such that the upconversion core was exposed (Scheme 1a and Fig. 1k, l). Finally, the
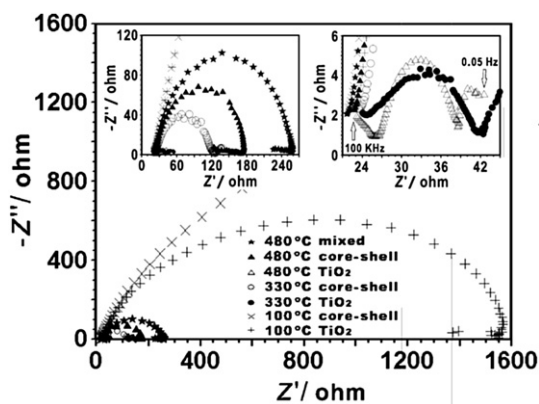
Fig. 5. AC impedance spectra of DSSCs based on bare FTO, pure TiO_2, $NaYF_4$:Yb^{3+},Er^{3+}/ TiO_2 core–shell and mixed PEs under 100 mW cm^{-2} illumination, initial E = open-circuit voltage of each cell, high freq = 100 kHz, low freq = 0.05 Hz, amplitude = 5 mV.
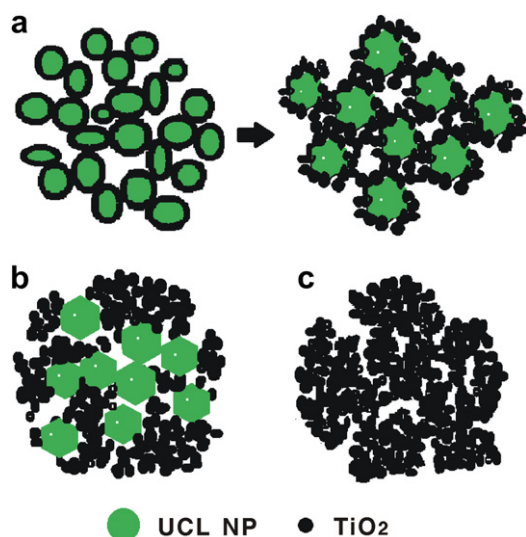
Scheme 1. Schematics of PEs based on the (a) NaYF$_4$:Yb^{3+},Er^{3+}/TiO$_2$ core—shell, (b) mixed and (c) pure TiO$_2$ NPs annealed at 480 °C.

structural evolution enhanced the fluorescence intensity of the material and extended the spectral response range of DSSCs to infrared radiation, which contributed to the enhancement of the DSSCs' efficiencies. In addition, the new core—shell structural design remained as the TiO$_2$ net structure of the PE (Scheme 1a and Fig. 1k, l) and resulted in a better capability of electron transfer, which was the same important factor for the enhancement of the DSSCs' efficiencies. For the mixed PE, however, the UCL NPs and TiO$_2$ NPs simply accumulated, and the connection between the semiconductor TiO$_2$ NPs was obstructed by the nonconductor UCL NPs, which blocked electron transfer (Scheme 1b and Fig. 5). For the pure TiO$_2$ PE, the infrared radiation was utilized to a much smaller degree because of the absence of UCL NPs, although its electron transfer properties were the best among all of the PEs because of the TiO$_2$ net structure (Fig. 5 and Scheme 1c). As a result, the upconversion core—shell structure is more effective for efficiency enhancement of DSSCs than either the simple mixed or the pure TiO$_2$ PE (Fig. 4 and Table 1).

4. Conclusions

In this work, novel upconversion NaYF$_4$:Yb^{3+},Er^{3+}/TiO$_2$ core—shell structure NPs were successfully synthesized and used as a PE in DSSCs. This core—shell structure material was composed of an upconversion NaYF$_4$:Yb^{3+},Er^{3+} core enwrapped by many TiO$_2$ NPs. This core—shell structure showed an excellent capacity to convert infrared to visible luminescence and retain semiconductor character, which was used to fabricate a more efficient DSSC as opposed to using pure TiO$_2$ NPs and a simple mixture. When using this specific core—shell structure, the NaYF$_4$:Yb^{3+},Er^{3+} core can absorb and utilize the infrared light, and at the same time, the TiO$_2$ shell net can effectively transmit the electrons in the PE; both improved the conversion efficiency of the DSSCs.

However, this single upconversion material still has some deficiencies, such as a narrowband emission spectrum, and its conversion efficiency has room for improvement. Perhaps if the core were doped with more rare earth elements, a larger spectral range could be utilized from the absorption of a wider spectrum of infrared light and efficient conversion to wideband visible light.

UCL materials can play a more important role in DSSCs, which will be the next focus of our research.

References

[1] A. Kumar, T.C. Kandpal, Energy 32 (2007) 861—870.
[2] B. O'Regan, M. Grätzel, Nature 353 (1991) 737—740.
[3] J. Zhang, X.X. Li, W. Guo, T.B.X. Hreid, J.F. Hou, H.Q. Su, Z.B. Yuan, Electrochimica Acta 56 (2011) 3147—3152.
[4] Q. Yao, J. Liu, Q. Peng, X. Wang, Y. Li, Chemistry — An Asian Journal 1 (2006) 737—741.
[5] Q.F. Zhang, G.Z. Cao, Nano Today 6 (2011) 91—109.
[6] H. Hafez, J. Wu, Z. Lan, Q. Li, G. Xie, J. Lin, M. Huang, Y. Huang, M.S.A. Abdel-Mottaleb, Nanotechnology 21 (2010) 415201/1—415201/6.
[7] J.C.G. Bünzli, S.V. Eliseeva, Journal of Rare Earths 28 (2010) 824—842.
[8] H. Hafez, M. Saif, M.S.A. Abdel-Mottaleb, Journal of Power Sources 196 (2011) 5792—5796.
[9] E. Downing, L. Hesselink, J. Ralston, R. Macfarlane, Science 273 (1996) 1185—1189.
[10] A. Shalav, B.S. Richards, T. Trupke, K.W. Kramer, H.U. Gudel, Applied Physics Letters 86 (2005) 013505/1—013505/3.
[11] J.F. Suyver, A. Aebischer, D. Biner, P. Gerner, J. Grimm, S. Heer, K.W. Kramer, C. Reinhard, H.U. Gudel, Optical Materials 27 (2005) 1111—1130.
[12] H.S. Mader, P. Kele, S.M. Saleh, O.S. Wolfbeis, Current Opinion in Chemical Biology 14 (2010) 582—596.
[13] F. Wang, D. Banerjee, Y. Liu, X. Chen, X. Liu, Analyst 135 (2010) 1839—1854.
[14] F. Wang, X.G. Liu, Chemical Society Reviews 38 (2009) 976—989.
[15] A. Aebischer, M. Hostettler, J. Hauser, K. Kramer, T. Weber, H.U. Gudel, H.B. Burgi, Angewandte Chemie International Edition 45 (2006) 2802—2806.
[16] J.F. Suyver, A. Aebischer, S. Garcia-Revilla, P. Gerner, H.U. Gudel, Physical Reviews B 71 (2005) 125123/1—125123/9.
[17] Y.J. Sun, Y. Chen, L.J. Tian, Y. Yu, X.G. Kong, J.W. Zhao, H. Zhang, Nanotechnology 18 (2007) 275609/1—275609/9.
[18] F. Wang, X.G. Liu, Journal of American Chemical Society 130 (2008) 5642—5643.
[19] K.A. Abel, J.C. Boyer, F.C.J.M. van Veggel, Journal of American Chemical Society 131 (2009) 14,644—14,645.
[20] Y. Wang, L.P. Tu, J.W. Zhao, Y.J. Sun, X.G. Kong, H. Zhang, Journal of Physical Chemistry C 113 (2009) 7164—7169.
[21] B. Dong, S. Xu, J. Sun, S. Bi, D. Li, X. Bai, Y. Wang, L.P. Wang, H.W. Song, Journal of Materials Chemistry 21 (2011) 6193—6200.
[22] D.S. Zhang, D. Zhao, K.Z. Zheng, N. Liu, W.P. Qin, Journal of Nanoscience and Nanotechnology 11 (2011) 9761—9764.
[23] K.A. Abel, J.C. Boyer, C.M. Andrei, F.C.J.M. van Veggel, The Journal of Physical Chemistry Letters 2 (2011) 185—189.
[24] G.S. Yi, G.M. Chow, Advanced Functional Materials 16 (2006) 2324—2329.
[25] W.B. Niu, S.L. Wu, S.F. Zhang, Dalton Transactions 40 (2011) 3305—3314.
[26] Z.Q. Ai, G.L. Sun, Q.L. Zhou, C.S. Xie, Journal of Applied Polymer Sciences 102 (2006) 1466—1470.
[27] T. Hirakawa, P.V. Kamat, Journal of American Chemical Society 127 (2005) 3928—3934.
[28] X.B. Chen, S.S. Mao, Chemical Reviews 107 (2007) 2891—2959.
[29] Z.P. Li, B.X. Ye, X.D. Hu, X.Y. Ma, X.P. Zhang, Y.Q. Deng, Electrochemical Communications 11 (2009) 1768—1771.
[30] M. Grätzel, Progress in Photovoltaics: Research and Applications 8 (2000) 171—185.
[31] F. Zhang, J. Li, J. Shan, L. Xu, D.Y. Zhao, Chemistry — An European Journal 15 (2009) 11,010—11,019.
[32] X.J. Kang, Z.Y. Cheng, C.X. Li, D.M. Yang, M.M. Shang, P.A. Ma, G.G. Li, N. Liu, J. Lin, Journal of Physical Chemistry C 115 (2011) 15,801—15,811.
[33] G.S. Yi, H.C. Lu, S.Y. Zhao, Y. Ge, W.J. Yang, D.P. Chen, L.H. Guo, Nano Letters 4 (2004) 2191—2196.
[34] L.J. Meng, C. Li, M.P. dos Santos, Journal of Inorganic and Organometallic Polymers and Materials 21 (2011) 770—776.
[35] K.H. Park, E.M. Jin, H.B. Gu, S.D. Yoon, E.M. Han, J.J. Yun, Applied Physics Letters 97 (2010) 023302/1—023302/3.
[36] Q. Wang, J.E. Moser, M. Grätzel, Journal of Physical Chemistry B 109 (2005) 14,945—14,953.